NITROGEN CYCLING

Rapid nitrous oxide cycling in the suboxic ocean

Andrew R. Babbin,[1,2]* Daniele Bianchi,[3] Amal Jayakumar,[1] Bess B. Ward[1]

Nitrous oxide (N_2O) is a powerful greenhouse gas and a major cause of stratospheric ozone depletion, yet its sources and sinks remain poorly quantified in the oceans. We used isotope tracers to directly measure N_2O reduction rates in the eastern tropical North Pacific. Because of incomplete denitrification, N_2O cycling rates are an order of magnitude higher than predicted by current models in suboxic regions, and the spatial distribution suggests strong dependence on both organic carbon and dissolved oxygen concentrations. Furthermore, N_2O turnover is 20 times higher than the net atmospheric efflux. The rapid rate of this cycling coupled to an expected expansion of suboxic ocean waters implies future increases in N_2O emissions.

Anthropogenically derived atmospheric N_2O concentrations increased over the past century (*1*–*3*), but the natural marine sources and sinks of N_2O have been difficult to quantify. Because of the paucity of direct measurements of N_2O production and consumption in the ocean, current rate estimates and predictions of how the N_2O budget will respond to a changing climate remain uncertain (*4*). The most concentrated oceanic sources of N_2O to the atmosphere are the suboxic (0 to 20 μmol l^{-1}) waters overlying the oxygen minimum zones (OMZs), based on measurements and models of supersaturated N_2O concentrations (*5*, *6*). Furthermore, N_2O is produced by both nitrification and denitrification, but the overall importance of each process is uncertain. Nitrification, the oxidation of ammonium to nitrite and further to nitrate, exhibits maximum rates just below the well-lit surface layer, where remineralization rates supplying ammonium are highest. Nitrification generates an N_2O by-product (*7*) whose yield is enhanced by suboxic concentrations—the yield of N_2O, as a fraction of nitrite production, can be as high as 10% in culture (*8*, *9*) and 0.4% in the environment (*10*, *11*). However, at very low (less than a few micromolar) oxygen concentrations, nitrification ceases (*12*), and no N_2O can be produced via this pathway.

Denitrification, the stepwise reductions of nitrate and nitrite through NO and N_2O to nitrogen gas, occurs in the ocean only when molecular oxygen is sufficiently low (less than 3 μmol l^{-1}) (*13*). This anaerobic process results in local N_2O minima within the OMZ core but has the potential to be a major N_2O source at the suboxic-anoxic interface (the oxycline) at the top of the OMZ. Over this narrow depth interval, N_2O consumption by the nitrous oxide reductase enzyme is inhibited by O_2 at an extent greater than its production in the denitrification sequence (*14*). Further, because the denitrification steps are predominantly heterotrophic, the rates are enhanced at shallow depths, where the supply of newly produced labile organic matter from the surface (*13*) is greater. Incomplete denitrification (reduction of NO_3^- to N_2O rather than to N_2) may account for a flux that is ignored or not explicitly represented in most biogeochemical ocean and climate models. Indeed, in culture experiments (*14*, *15*) and sediment incubations (*16*) at suboxic but nonzero O_2 concentrations, denitrification activity decreased as expected with increasing O_2 concentrations, but the N_2O yield (i.e., the proportion of denitrification halting at N_2O) increased to ~50% (*15*).

We directly measured the reduction of N_2O to dinitrogen gas by using labeled isotopic $(^{15}N)_2O$ tracer incubation experiments at three stations in the eastern tropical North Pacific (ETNP), the largest suboxic zone (*17*) and a major site of N_2O production (*18*, *19*). N_2O reduction is the only major biological N_2O consumption process; because production occurs via multiple pathways, in situ production rates via isotopic tracer techniques cannot be directly constrained (*20*).

The transect across the ETNP (fig. S1) showed the characteristic features associated with OMZs, namely a N_2O concentration peak (~100 nmol l^{-1}) at the base of a steep oxygen gradient and an N_2O concentration minimum in the core of the OMZ. All three sites displayed similar alignments of oxygen, N_2O, and nitrite maxima and minima (Fig. 1A), indicating similar mechanisms affecting the biogeochemistry across the region. The similarity between the N_2O profile at the offshore station 2 and data from a nearby site measured 12 years prior (*19*) (Fig. 1B) indicates long-term stability in the shape and peak magnitudes of the N_2O profiles.

N_2O consumption rates (Fig. 2) measured across all three profiles were up to 35 nmol l^{-1} day^{-1}, indicating residence times as low as 1 day (calculated from the concentration divided by the biological rate). This fast turnover was observed throughout the OMZ core, presumably because of tight coupling of sequential denitrification steps. Within the oxycline, the N_2O residence times increased and the reduction rates decreased sharply as O_2 increased. This synchronism is consistent with oxygen poisoning of the nitrous oxide reductase enzyme above the OMZ. Moreover, and of greater consequence to atmospheric N_2O emissions, an estimate of the rate of production based on a one-dimensional (1D) transport-reaction balance (fig. S3) was systematically larger than that of consumption near the base of the oxycline. This 1D estimate is likely to be conservative, because the inclusion of horizontal transport terms, which act to erode the N_2O peak, would require an increase in the N_2O source to maintain the balance (table S2 and supplementary text). The observed near-shore (station 1) rates of N_2O reduction and production decreased with depth (Fig. 2), resembling the depth-dependent power law decay of organic carbon supply (*13*). This organic carbon dependence of N_2O cycling was also apparent from the occurrence of the highest rates near shore, where the greatest primary production occurs. These measurements highlight the large spatial heterogeneity of N_2O cycling dependent on organic carbon export in the ETNP.

We investigated the broader implications of such rapid N_2O cycling with a mechanistic, 1D model of OMZ biogeochemistry (supplementary materials) built on parameterizations widely adopted in ocean biogeochemical models, including biological N_2O production via nitrification, enhanced at suboxic concentrations (*4*, *6*, *21*, *22*), and consumption via denitrification (*19*). Following previous parameterizations (*21*), we defined an oxygen threshold of 2 μmol l^{-1}, above which N_2O was produced and below which, consumed. However, this 1D model with N_2O production from nitrification alone generated a production rate (maximum of 0.3 nmol l^{-1} day^{-1}) that was a fraction of the net production rate calculated from the measured consumption (Fig. 3A). The observed N_2O concentration peaks measured here at >100 nmol l^{-1} (Fig. 1) are likely not reproduced in models (*21*), including our 1D version (which only achieves a maximum of 70 nmol l^{-1}), because they do not include explicit production by incomplete denitrification. The importance of denitrification to N_2O production has been implicated by measurements across all three major OMZs: the ETNP (*18*, *23*), the eastern tropical South Pacific (ETSP) (*24*), and the Arabian Sea (*20*, *25*).

We expanded the 1D model to separate the N_2O production and consumption terms of denitrification and allow for O_2-dependent decoupling (*26*). With this change, denitrification became a major N_2O source in the low-O_2 waters directly overlying the OMZ (9.3 μmol m^{-2} day^{-1}) and was comparable in size to the source from nitrification (9.1 μmol m^{-2} day^{-1}). Furthermore, the maximum modeled net N_2O production rate of 0.6 nmol l^{-1} day^{-1} is consistent with our observations (Fig. 3B), with a peak concentration of >110 nmol l^{-1}. Such agreement could not be achieved with production via nitrification alone and suggests that denitrification constitutes a major and largely overlooked source of N_2O. This conclusion also holds for a range of model parameters and formulations, including a simple

[1]Department of Geosciences, Princeton University, Princeton, NJ 08544, USA. [2]Department of Civil and Environmental Engineering, Massachusetts Institute of Technology, Cambridge, MA 02139, USA. [3]School of Oceanography, University of Washington, Seattle, WA 98105, USA.
*Corresponding author. E-mail: babbin@mit.edu

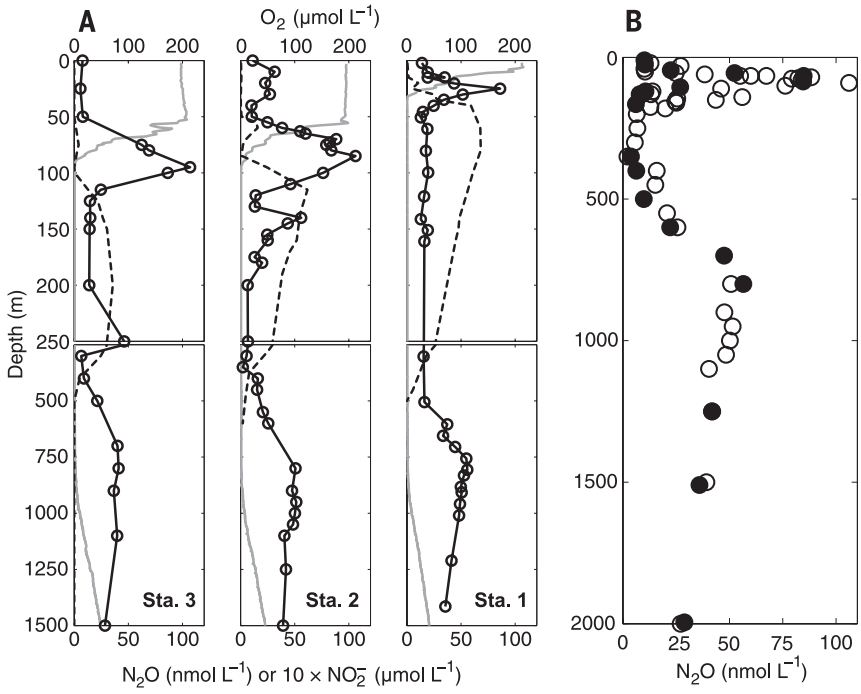

Fig. 1. Biogeochemical measurements. (**A**) Depth profiles of N_2O (open circles), O_2 (solid gray line), and NO_2^- (dashed line) concentrations at the three stations included in this study. (**B**) Comparison of N_2O concentration data (open circles) from station 2 collected in April 2012 with those from a previous study (*19*) (solid circles) of a nearby location (16°N 107°W) in spring 2000.

representation of lateral transports, as shown by a series of sensitivity studies (fig. S2, table S2, and supplementary text).

Similar to the model results, a conservative average from offshore measurements at the base of the oxycline indicated a net production rate on order of ~1 nmol l^{-1} day^{-1}. Based on the measured rates and the observed extent of the suboxic layer at the base of the oxycline of the three profiles, production exceeds consumption across a thickness of ~10 ± 4 m (SD) immediately overlying the anoxic layer. A 1 nmol l^{-1} day^{-1} imbalance integrated over 10 m equates to an air-sea N_2O flux of 10 μmol m^{-2} day^{-1}, which is comparable (30 to 100%) to the fluxes estimated in the analogous suboxic ETSP (*24*). Our model including a denitrification N_2O source produced a similar atmospheric efflux of 13 μmol m^{-2} day^{-1}. As an order-of-magnitude estimate, integrating a 10 μmol m^{-2} day^{-1} flux horizontally over the extent of the suboxic ETNP ($25.7 \times 10^{12} \pm 1.5 \times 10^{12}$ m^2) yields a net atmospheric N_2O flux out of the ETNP OMZ of 1.3 ± 0.1 Tg of N $year^{-1}$. Furthermore, if we conservatively estimate the average reduction rate based on our measurements within the ETNP OMZ (2 nmol l^{-1} day^{-1}) and integrate over the full volume of the anoxic ETNP OMZ ($1.2 \times 10^{15} \pm 0.5 \times 10^{15}$ m^3), the total cycling rate through N_2O is 25 ± 10 Tg of N $year^{-1}$, or 20 times higher than the net efflux. This gross rate of N_2O generation is comparable to previous estimates of denitrification rates from the ETNP (*27*–*30*). Because the net outgassing of N_2O to the atmosphere results from the residual between large production and reduction rates, it could change greatly in response to even a small decoupling of production and consumption, caused, for example, by more frequent O_2 injections (*31*) or changes in the volume and geometry of suboxic zones (*32*, *33*).

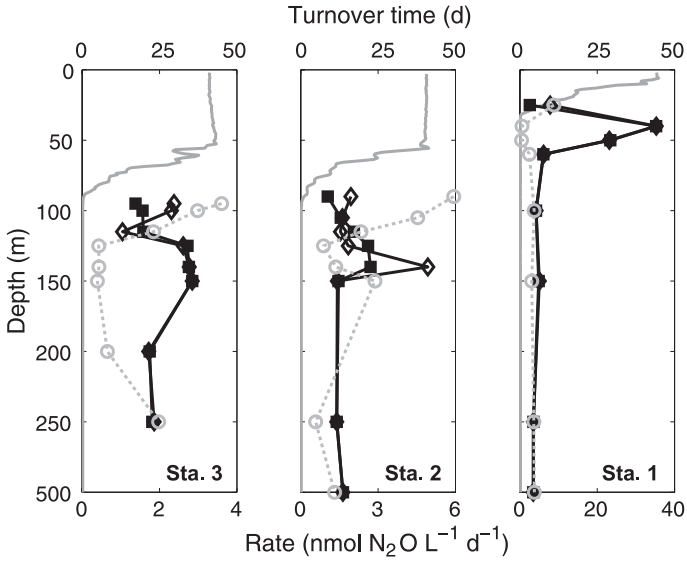

Fig. 2. N_2O cycling rates. Rates of measured N_2O consumption (solid squares) and calculated production (open diamonds) are shown at the three stations. Turnover times are indicated by open circles. Scaled (0 to 100% saturation) O_2 concentration profiles (solid gray line) are included for reference (see Fig. 1 for concentrations). Note the broken vertical axis between 250 and 500 m. N_2O production was calculated by using the measured consumption rates and concentration profiles and assuming a vertical balance between advection, diffusion, consumption, and production. Lateral transport processes, which would tend to erode the N_2O peak and thus require more production, were ignored here, making these production rates likely lower estimates (supplementary text).

Our results show that the net accumulation of N_2O in the OMZs on the multiyear time scales dictated by ocean circulation hides the delicate balance between production and consumption that proceeds on time scales at least one order of magnitude faster. Over long time scales into the future, expanding and shoaling OMZs resulting from changes in physical circulation, widespread ocean deoxygenation (*34*), and increased fertilizer runoff stimulating phytoplankton blooms could exacerbate marine N_2O accumulation and outgassing (*4*, *31*). This increase would be especially important given the rapid biological rates measured in the ETNP. The rapid turnover of N_2O in OMZs also implies that shorter time scale variations influence N_2O

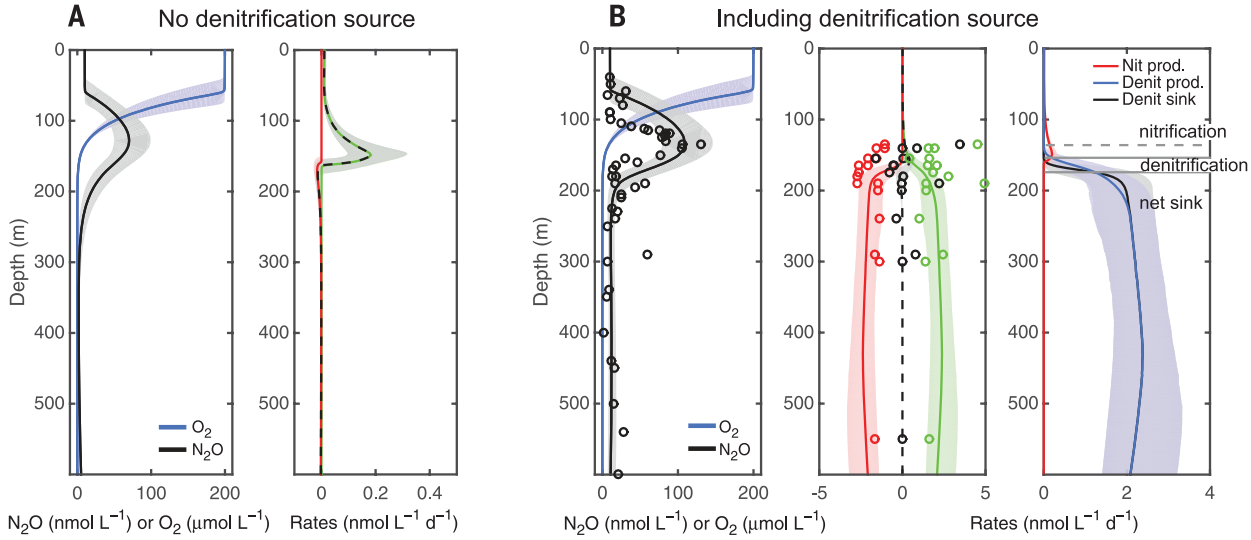

Fig. 3. One-dimensional model of N_2O cycling in the OMZ. (**A**) Modeled N_2O and O_2 concentrations using a mechanistic 1D model of OMZ biogeochemistry, with rates of production from nitrification (green) and consumption from denitrification (red). The net rate is given by the dashed black curve. (**B**) As in (A) but with an additional N_2O source from denitrification included. The third graph separates the different production and consumption terms. Points show measurements at stations 2 and 3. Model and data profiles have been shifted vertically to align the N_2O peaks to the mean model N_2O peak depth. Solid horizontal gray lines separate the layers of nitrification-dominated production, denitrification-dominated production, and net denitrification consumption. The dashed gray line shows where denitrification begins to act as a major N_2O source in the model. Envelopes in all graphs show the standard deviation from an ensemble of Monte Carlo runs (N = 5000) simultaneously varying all of the parameterizations.

flux, as reported for the Arabian Sea's annual monsoons (*35*). El Niño–Southern Oscillation strongly affects the mixed layer and thermocline depths and surface productivity in the eastern tropical Pacific. Via this natural variability, the OMZs of the ETNP and the ETSP should expand and shoal during a La Niña and contract during an El Niño (*36*).

Current estimates of the marine N_2O sources to the atmosphere that do not mechanistically account for incomplete denitrification, including the Intergovernmental Panel on Climate Change (IPCC) estimate of ~4 Tg of N year^{-1}, are low considering the overall denitrification rates to N_2 in the OMZs (*33*, *35*, *37*). If we assume that the three major OMZs are approximately equivalent, the N_2O production rates predicted here would account for 4 Tg of N year^{-1} from the OMZs alone. This is a conservative analysis, limited to the offshore sites and ignoring the coastal region with higher rates and imbalances (Fig. 2). Inclusion of coastal sites could substantially increase this estimate. Further, models parameterizing N_2O production via only nitrification require tuning by some additional suboxic process to produce N_2O in the OMZs and better simulate concentration distributions (*4*, *22*, *38*). The directly measured rates and simple model presented in this paper show that these tunings do not capture the dynamics necessary to represent accurately marine N_2O cycling.

REFERENCES AND NOTES

1. J. Flückiger *et al.*, *Science* **285**, 227–230 (1999).
2. A. R. Ravishankara, J. S. Daniel, R. W. Portmann, *Science* **326**, 123–125 (2009).
3. G. Myhre *et al.*, in *Climate Change 2013: The Physical Science Basis. Contribution of Working Group I to the Fifth Assessment Report of the Intergovernmental Panel on Climate Change*, T. F. Stocker *et al.*, Eds. (Cambridge Univ. Press, Cambridge, 2013), pp. 659–740.
4. J. Martinez-Rey, L. Bopp, M. Gehlen, A. Tagliabue, N. Gruber, *Biogeosciences Discuss.* **11**, 16703–16742 (2014).
5. Y. Cohen, L. I. Gordon, *J. Geophys. Res. Oceans* **84**, 347–353 (1979).
6. P. Suntharalingam, J. L. Sarmiento, *Global Biogeochem. Cycles* **14**, 429–454 (2000).
7. A. E. Santoro, C. Buchwald, M. R. McIlvin, K. L. Casciotti, *Science* **333**, 1282–1285 (2011).
8. T. J. Goreau *et al.*, *Appl. Environ. Microbiol.* **40**, 526–532 (1980).
9. F. Lipschultz *et al.*, *Nature* **294**, 641–643 (1981).
10. J. W. Elkins, S. C. Wofsy, M. B. McElroy, C. E. Kolb, W. A. Kaplan, *Nature* **275**, 602–606 (1978).
11. H. P. J. de Wilde, M. J. M. de Bie, *Mar. Chem.* **69**, 203–216 (2000).
12. W. Martens-Habbena, P. M. Berube, H. Urakawa, J. R. de la Torre, D. A. Stahl, *Nature* **461**, 976–979 (2009).
13. A. R. Babbin, R. G. Keil, A. H. Devol, B. B. Ward, *Science* **344**, 406–408 (2014).
14. H. Körner, W. G. Zumft, *Appl. Environ. Microbiol.* **55**, 1670–1676 (1989).
15. M. R. Betlach, J. M. Tiedje, *Appl. Environ. Microbiol.* **42**, 1074–1084 (1981).
16. K. S. Jørgensen, H. B. Jensen, J. Sørensen, *Can. J. Microbiol.* **30**, 1073–1078 (1984).
17. A. Paulmier, D. Ruiz-Pino, *Prog. Oceanogr.* **80**, 113–128 (2009).
18. N. Yoshida, A. Hattori, T. Saino, S. Matsuo, E. Wada, *Nature* **307**, 442–444 (1984).
19. H. Yamagishi *et al.*, *J. Geophys. Res. Biogeosciences* **112**, G02015 (2007).
20. J. C. Nicholls, C. A. Davies, M. Trimmer, *Limnol. Oceanogr.* **52**, 156–168 (2007).
21. C. Nevison, J. H. Butler, J. W. Elkins, *Global Biogeochem. Cycles* **17**, 1119 (2003).
22. X. Jin, N. Gruber, *Geophys. Res. Lett.* **30**, 2249 (2003).
23. T. Yoshinari *et al.*, *Mar. Chem.* **56**, 253–264 (1997).
24. L. Farías *et al.*, *Limnol. Oceanogr.* **54**, 132–144 (2009).
25. S. W. A. Naqvi *et al.*, *Proc. Indian Acad. Sci. Earth Planet. Sci.* **107**, 367–378 (1998).
26. T. Dalsgaard *et al.*, *MBio* **5**, e01966-e14 (2014).
27. C. Deutsch, N. Gruber, R. M. Key, J. L. Sarmiento, A. Ganachaud, *Global Biogeochem. Cycles* **15**, 483–506 (2001).
28. D. Bianchi, J. P. Dunne, J. L. Sarmiento, E. D. Galbraith, *Global Biogeochem. Cycles* **26**, GB2009 (2012).
29. T. DeVries, C. Deutsch, F. Primeau, B. Chang, A. Devol, *Nat. Geosci.* **5**, 547–550 (2012).
30. T. DeVries, C. Deutsch, P. A. Rafter, F. Primeau, *Biogeosciences* **10**, 2481–2496 (2013).
31. L. A. Codispoti, *Science* **327**, 1339–1340 (2010).
32. L. Stramma, G. C. Johnson, J. Sprintall, V. Mohrholz, *Science* **320**, 655–658 (2008).
33. S. W. A. Naqvi *et al.*, *Nature* **408**, 346–349 (2000).
34. R. F. Keeling, A. Körtzinger, N. Gruber, *Annu. Rev. Mar. Sci.* **2**, 199–229 (2010).
35. H. W. Bange *et al.*, *Atmos. Chem. Phys.* **1**, 61–71 (2001).
36. T. Ito, C. Deutsch, *Global Biogeochem. Cycles* **27**, 1119–1128 (2013).
37. H. W. Bange, *Atmos. Environ.* **40**, 198–199 (2006).
38. P. Suntharalingam *et al.*, *Geophys. Res. Lett.* **39**, L07605 (2012).

ACKNOWLEDGMENTS

We thank the captain and crew of the R/V *Thomas G. Thompson* and chief scientist A. H. Devol for assistance in sampling and A. Morello and X. Peng for help with nitrite and N_2O measurements, respectively. J. L. Sarmiento provided valuable inputs in the development of the oxygen minimum zone model. This work was funded by a National Defense Science and Engineering Graduate Fellowship to A.R.B., NSF grant no. 1029951 to B.B.W. and A.J., and University of Washington funding to D.B. A.R.B. was additionally supported by a NSF Postdoctoral Research Fellowship in Biology (no. 1402109) while preparing the paper. All data measurements presented in this paper are included in table S3. The 1D MATLAB model code and output are available in the supplementary materials. A.R.B. and B.B.W. designed and conducted the shipboard experiments and analysis, D.B. designed and implemented the 1D model, and A.J. measured N_2O concentrations. All authors analyzed the data and model results and wrote the paper.

SUPPLEMENTARY MATERIALS

www.sciencemag.org/content/348/6239/1127/suppl/DC1
Materials and Methods
Supplementary Text
Figs. S1 to S3
Tables S1 to S3
References (*39*–*53*)
Supplementary Data

12 February 2015; accepted 28 April 2015
10.1126/science.aaa8380

Science
AAAS

Rapid nitrous oxide cycling in the suboxic ocean
Andrew R. Babbin *et al.*
Science **348**, 1127 (2015);
DOI: 10.1126/science.aaa8380

Science (print ISSN 0036-8075; online ISSN 1095-9203) is published weekly, except the last week in December, by the American Association for the Advancement of Science, 1200 New York Avenue NW, Washington, DC 20005.